



Biomechanics of the Total Ankle Arthroplasty: Stress Analysis and Bone Remodeling



Daniela Rodrigues

Integrated Master in Biomedical Engineering
Instituto Superior Técnico, Lisbon, Portugal
danielasrodrigues@ist.utl.pt

Abstract – The total ankle arthroplasty (TAA) is an alternative procedure to the arthrodesis in the treatment of advanced arthritis in the ankle joint. However, the total ankle prostheses are not yet widely accepted and do not have the same success rate of the hip, knee or even shoulder prostheses. Thus, the aim of this work is the development of a finite element (FE) model of the ankle joint complex (AJC) in order to study the influence of two different prostheses, Agility™ (considering two different designs) and S.T.A.R.™, on the stress distribution and bone remodeling. This work involved the geometric and FE modeling of the AJC and the prostheses, Agility™ and S.T.A.R.™. Subsequently, the models simulating the TAA were created. Then, stress analysis was performed, and the bone remodeling model developed in IDMEC/IST was used to determine the bone density distribution in the talus and tibia. The results indicated that the new design of Agility™ prosthesis has better performance than the old design. However, both prostheses (especially Agility™) exceeded the contact stress recommended for the intermediate/polyethylene component (10 MPa). Moreover, after the insertion of both prostheses, the stresses increased near the resected surface in the talus, which may contribute to early loosening and subsidence of the talar component. Regarding the bone remodeling analysis, both prostheses showed evidences that may lead to stress shielding effect. In conclusion, these prostheses still have some untested features and the optimal configuration is currently not known.

Key-words: Biomechanics, Ankle joint complex, Total ankle arthroplasty, Finite element method, Bone remodeling

1. Introduction

The ankle has unique anatomical, biomechanical and cartilaginous structural characteristics that allow the joint to withstand the very high mechanical stresses and strains during walking, running and other activities [1]. The most common pathology that can disrupt ankle's function is arthritis, which involves the destruction of the articular cartilage. Although arthritis predominantly affects the joints of the hip and knee and the exact prevalence of ankle arthritis is difficult to quantify, in 2005 there were about 538000 people affected by arthritis in the foot/ankle only in the USA [2]. Moreover, this number is expected to increase in the following years worldwide. At present, most types of arthritis cannot be cured but some treatments have been developed [3]. Those treatments encompass both non- and surgical

measures. However, non-surgical measures have been shown to have only small effects on pain relief, and when those treatments fail, surgical measures are required. The most effective surgical measures are ankle arthrodesis and total ankle arthroplasty (TAA). Arthrodesis is the artificial induction of joint ossification between bones. It has been the so-called "gold standard" for the treatment of end-stage ankle arthritis, providing pain relief to the patients [4]. However, this procedure is far from the ideal one since the joint and thus the mobility provided by the joint are eliminated. On the other hand, arthroplasty is the replacement of an arthritic or injured joint with an artificial joint (prosthesis). This procedure is not only aimed at relieving pain but also restoring mobility, stability and integrity of the joint, which challenges the idea that arthrodesis is the best treatment for ankle arthritis [5]. Inspired by the success of the total hip and knee arthroplasties, there was an interest in TAA and the first generation prostheses were introduced in the 1970s. The short and intermediate term results of the TAAs were satisfactory, but the long-term results were disappointing, and TAA was largely abandoned due to poor survivorship [6]. Then, in the late 1980s and early 1990s there was a renewed interest in TAA with the introduction of the second generation of total ankle prostheses which more closely replicated the natural anatomy and mobility of the ankle, giving rise to improved clinical outcomes with mid-term follow-up [7-13]. Since then, a more profound understanding of ankle biomechanics has led to the development of new modern total ankle prostheses [4]. Nevertheless, TAA is still seen as an inferior procedure to arthrodesis by many in the orthopaedic community [14-17]. In fact, the total ankle prostheses are not yet widely accepted and do not have the same or even similar success rate of the total hip, knee or even shoulder prostheses [18]. One of the main reasons for that may be the fact that the ankle is the last joint in the lower limb in which total arthroplasty was attempted and therefore the amount of research and development time dedicated to it has lagged behind that of the hip and knee [17]. After an exhaustive literature review it was possible to confirm that many finite element (FE) models were created for hip, knee and some for shoulder simulating total or partial replacement surgeries, but very few can be found for TAA or even to the intact ankle joint. Furthermore, FEM has been widely used in hip, knee and shoulder

to investigate time-dependent biological processes in tissues, such as bone remodeling process. However, regarding the bone remodeling process in the ankle joint, only one study can be found in literature [19].

Thus, the aim of this work is the development of a FE model of the ankle joint complex (AJC) in order to study the influence of two different prostheses, Agility™ and S.T.A.R.™, on the stress distribution and bone remodeling after a TAA. This is done using the FEM provided by the commercial software ABAQUS® together with the model of bone remodeling developed in IDMEC/IST.

2. Background

2.1. Anatomy

The human foot has three main joints namely the talocrural joint (well-known as the ankle joint), the talocalcaneal joint (well-known as the subtalar joint) and the midtarsal joints. The ankle joint is formed by the inferior extremity of the fibula and tibia, and the dorsum of the talus. The subtalar joint consists of the talus and calcaneus whereas the midtarsal joints are formed by the calcaneocuboid and talonavicular articulations [20]. In general several authors [21, 22] describe the AJC as being constituted by the ankle and subtalar joints. However, sometimes another joint is also described as part of the AJC namely the distal tibiofibular joint, which is formed by the inferior extremities of the fibula and tibia. In the present work it was considered the AJC as being constituted by the ankle, subtalar and distal tibiofibular joints. However, it is important to mention that the main object of study in this work is the ankle joint.

2.2. Total Ankle Prostheses

The search for a workable total ankle prosthesis design has taken many different approaches.

In first generation of the total ankle prostheses there were only constrained/congruent and unconstrained/incongruent prostheses. In order to overcome the problems reported for those prostheses, it was introduced an intermediate component between the tibial and talar components that works like a bearing. This intermediate component helps to absorb the forces passing through the tibia and fibula and distributing them to the talus, and this way allowing almost normal ankle motion after TAA [23]. Taking this new concept into account, the second generation prostheses started to be of the semiconstrained type (two-component, fixed-bearing designs, such as Agility™) and afterwards were also designed to be at the same time minimally constrained and congruent (three-component, mobile-bearing designs, such as S.T.A.R.™) [1, 24].

2.3. Bone Remodeling Model

The model used in the present work is based on a topology optimization criterion for 3-D linear elastic bodies in contact. It is an extension of the model developed by Fernandes *et al.* in [25, 26], with the equilibrium equation expressed for the contact problem being introduced by Folgado *et al.* [27, 28]. A porous material with a periodic microstructure is obtained by the repetition in space of a cubic cell with rectangular holes (open cell) [27], whose dimensions are characterized by a_1, a_2, a_3 . At each point, bone is characterized by both the parameters of the microstructure, $\mathbf{a} = (a_1, a_2, a_3)^T$, that define the relative density, and the orientation of the cell, using the Euler angles (θ) [27]. In particular, the relative density is calculated by $\mu = 1 - a_1.a_2 - a_2.a_3 - a_1.a_3 + 2 a_1.a_2.a_3$, for $a_i \in [0,1]$, $i=1,2,3$. This way, $a_i = 1$ (for $i=1,2,3$) corresponds to the absence of bone ($\mu = 0$) whereas $a_i = 0$ (for $i=1,2,3$) corresponds to cortical bone ($\mu = 1$). In conclusion, maximum relative density values correspond to cortical bone whereas intermediate values correspond to trabecular bone. The equivalent elastic properties of the material are obtained using the method of homogenization [29]. Using a multiple loading criterion that considers different load conditions at different temporal instants, the optimal topology is obtained by minimizing the work of the applied forces, which in turn maximizes the overall stiffness of the structure. This is influenced by an additional term, k , that is related to the biological cost of the organism in maintaining bone homeostasis. The bone remodeling law is given by:

$$\sum_{P=1}^{NC} \left(\alpha^P \frac{\partial E_{ijkl}^H}{\partial \mathbf{a}} e_{kl}(\mathbf{u}^P) e_{ij}(\mathbf{v}^P) \right) - k \frac{\partial \mu^m}{\partial \mathbf{a}} = 0 \quad (1)$$

where NC is the number of applied load cases, α^P are the load weight factors satisfying $\sum_{P=1}^{NC} \alpha^P = 1$, E_{ijkl}^H are the homogenized material properties, e_{ij} and e_{kl} are the components of the strain field and \mathbf{u}^P is the set of displacement fields. The parameters k and m , which define the cost of bone maintenance, and, therefore, control the total amount of bone mass, depend on several biological factors such as gender, age, hormonal status and disease.

3. Computational Modeling

3.1. Geometric Modeling of the Bones

The 3-D solid models of each intact bone, namely tibia, fibula, talus and calcaneus, were obtained from the VAKHUM project [30]. Then, in order to obtain a smoother and more natural and simple surface for each bone, a sequence of filters was applied to each bone, using the software ParaView. Then, all the bones were imported to SolidWorks® and their assembly was performed. Additionally, it was also incorporated in the model the cartilage of each bone and the interosseous membrane. Moreover, there is no need to have the superior extremity of the tibia and

fibula in the model since the prosthesis is placed in the inferior extremity of the tibia and in the dorsum of the talus, and so the changes in stress distribution and bone density after a TAA occur mainly in the areas adjacent to the prosthesis. Thus, a cut was performed through the middle of the tibia and fibula.

3.2. Geometric Modeling of the Prostheses

Subsequently, the solid models of the Agility™ and S.T.A.R.™ prostheses were developed based on informative documents provided by the DePuy Orthopaedics, Inc. [31] and Small Bone Innovations, Inc. [32] companies, respectively. This was done using SolidWorks®.

3.3. Assembly of the Models – Virtual Surgical Procedure

When a TAA is performed, the ankle joint's articular surfaces are resected and then replaced with specially designed prosthetic components. Thus, the intention at this stage was to create the models in which the ankle joint's articular surfaces are substituted by prosthetic components, which may be termed by virtual surgical procedure. This procedure was performed for Agility™ and S.T.A.R.™ prostheses, and based on surgical technique manuals provided by the DePuy Orthopaedics, Inc. [33] and Small Bone Innovations, Inc. [34] companies, respectively. Moreover, this procedure was also performed according to what was advised by Dr. Nuno Ramiro (experienced orthopaedic surgeon) and Prof. Dr. Jacinto Monteiro (experienced orthopaedic surgeon, external supervisor of this work), both of whom clinical collaborators from Faculty of Medicine of the University of Lisbon.

As result, the models of the intact AJC, and after the insertion of the Agility™ and S.T.A.R.™ prostheses were created (see Figure 1). During this work, the models after the insertion of the Agility™ and S.T.A.R.™ prostheses are called TAA+Agility™ and TAA+S.T.A.R.™, respectively.

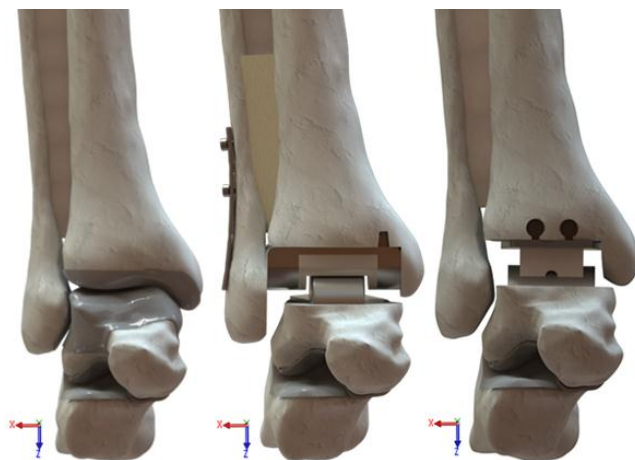


Figure 1 The intact model (at left), the TAA+Agility™ model (at middle) and the TAA+S.T.A.R.™ model, (at right). Software used: SolidWorks®.

3.4. FE Modeling

The three models under study (intact, TAA+Agility™ and TAA+S.T.A.R.™) were imported from the SolidWorks® to ABAQUS® and then eight major ligaments of the AJC were included in each model. This choice was based on the studies of Reggiani *et al.* [35] and Corazza *et al.* [36], which in turn took into account the study of Pankovich and Shivaram [37]. Each of these eight ligaments was modeled as a tension-only truss element.

Initially, for the stress analysis, the bone was considered linearly elastic, heterogeneous (divided in cortical and trabecular bone) and isotropic. Afterwards, for the bone remodeling analysis, the bone was modeled as a cellular material with an orthotropic microstructure, in which the relative density can vary along the domain and is given by the material optimization process, i.e., it results from the solution of the optimization problem. The constituent materials of all other structures were considered isotropic with linear elastic behaviour, whose properties are shown in Table 1.

Table 1 Material properties defined in the three models under study (intact, TAA+Agility™ and TAA+S.T.A.R.™).

Component	Material	Young's modulus, E (MPa)	Poisson's ratio, ν
Cortical Bone [38, 39]		19000	0.3
Trabecular Bone [40]		500	0.3
Cartilage [41]		1	0.4
Interosseous Membrane		99.5*	0.5*
Bone Graft		200**	0.3**
Plate and Screws (Agility™)	Ti [42]	110000	0.33
Tibial component (Agility™)	Ti [42]	110000	0.33
Polyethylene component (Agility™)	UHMWPE [43]	557	0.46
Talar component (Agility™)	Co-Cr [42]	193000	0.29
Tibial component (S.T.A.R.™)	Co-Cr-Mo [19]	210000	0.3
Polyethylene component (S.T.A.R.™)	UHMWPE [43]	557	0.46
Talar component (S.T.A.R.™)	Co-Cr-Mo [19]	210000	0.3

* Not found in literature, it was assumed to be similar to the ligament with smaller stiffness

** Not found in literature, it was assumed to be similar but weaker than trabecular bone

To simulate the surface interactions among the cartilages, the automated surface-to-surface contact algorithm provided by ABAQUS® was used. Due to the lubricating nature of these articular surfaces, the contact behaviour between them can be considered almost frictionless [44] (the coefficient of friction of 0.01 was used [45]). Also, the surface interactions between the cartilage and bone were naturally considered rigidly bonded (tied), as well as the interactions between the interosseous membrane and bones (fibula and tibia). Assuming a successful fixation of both prostheses (Agility™ and S.T.A.R.™) on bone, the surface interactions between both tibial and talar components and bone was considered rigidly bonded (tied). Regarding the surface interactions among the prosthetic components, it was defined again a surface-to-surface contact behaviour,

and the friction coefficient between the talar and polyethylene components (for both prostheses) and between the tibial and polyethylene components (only for S.T.A.R.[™] prosthesis) was defined to be 0.04, according to [35]. Moreover, for the TAA+Agility[™] model, the surfaces interactions between the bone graft and bones (fibula and tibia) were considered rigidly bonded (tied), as well as the interactions “screw-bone” and “plate-bone”. The two screws were also rigidly bonded to the plate.

The applied loading conditions used in this work were based on the data provided in [35] (Table 2).

Table 2 Loading conditions used in this work according to the position (D – Dorsiflexion; N – Neutral; P – Plantarflexion).

Position	D (-10°)	N (0°)	P (+15°)
Concentrated Force (N)			
Axial force	1600	600	400
Interior-exterior force	185	-150	-100
Anterior-posterior force	-185	-280	-245
Moment (N)			
Interior-exterior torque	6.2	2.85	-0.1

Three different static load cases were applied to each model (intact, TAA+Agility[™] and TAA+S.T.A.R.[™]), according to the dorsiflexion, neutral and plantarflexion positions. Regarding the bone remodeling analysis, the three load cases were included in the same computer simulation (considering the three positions under study at once), using the multiple load criteria with equal weights (1/3). For the stress analysis, each of the three load cases was considered individually for each model according to the position. Moreover, for the stress analysis, another two loading conditions were included in this work. Firstly, an axial force of 600 N was applied to the three positions. Then, the axial forces of 1600 N, 600 N and 400 N were applied to dorsiflexion, neutral and plantarflexion positions, respectively. Regarding the boundary conditions, the calcaneus was fixed in three parts.

Due to the limitation for the automatic-meshing algorithms in ABAQUS[®] to produce hexahedral meshes, 4-noded tetrahedral elements were used for meshing all the constituent parts of the three models under study. The resulting FE meshes for the three models under study are shown in Figure 2.

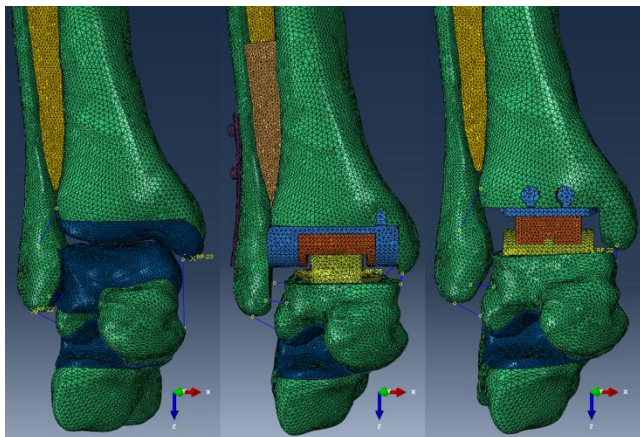


Figure 2 FE meshes for the three models under study: intact (at left), TAA+Agility[™] (at middle) and TAA+S.T.A.R.[™] (at right).

4. Results and Discussion

4.1. Contact Stress Distribution in the Intact Ankle Joint

The contact stress distribution in the articular surfaces is commonly used to validate FE models, which is a very important step before any further investigation. Thus, the comparison between experimental and FE results obtained by other authors and the present FE results could help establishing the validity of the present computational model.

The FE-computed contact stresses in the ankle joint for dorsiflexion, neutral and plantarflexion positions are displayed on the cartilages of the intact tibia and talus, in Figure 3. Three loading conditions were considered in this study. At first, only an axial load was included aiming to compare the results with the available studies in the literature that included the same loading condition. In one case, the axial load of 600 N was applied to the three positions (Figure 3). In the other case, the axial loads of 1600 N, 600 N and 400 N were applied to dorsiflexion, neutral and plantarflexion positions, respectively (not shown here). Then, the contact stresses for the same three positions and including all components of the concentrated force and the internal-external torque were also computed (not shown here). For reasons of synthesis, only the results when considering an axial force of 600 N to the three positions are shown.

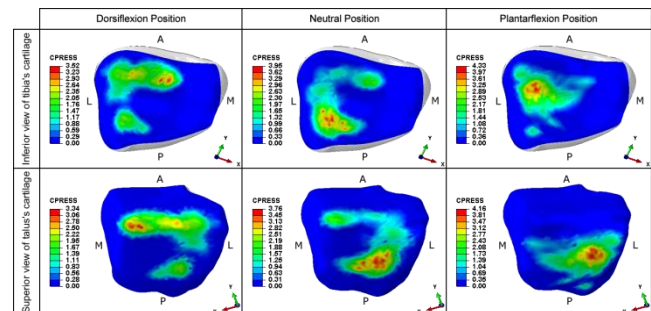


Figure 3 Inferior and superior views of the tibia and talus's cartilages, respectively, overlaid with FE-computed contact stresses (MPa) for the dorsiflexion, neutral and plantarflexion positions, considering only an axial force of 600 N to the three positions. Legend: A – Anterior; P – Posterior; L – Lateral; M – Medial. Software used: ABAQUS[®].

For the contact area only a qualitative analysis was performed while for the contact stress a quantitative analysis was accomplished. The maximum and mean FE-computed contact stresses in the tibial surface for the three loading conditions are summarized in Table 3. The qualitative analysis of the contact area showed that, compared with neutral position, in dorsiflexion there was a slight increase in the contact area while in plantarflexion there was a decrease in the contact area, which was also reported in [46]. Moreover, in the three loading conditions, the contact stresses spanned most of the lateral half of the tibial and talar surfaces, which was also reported in [47]. Besides not shown here, it was also observed an increasing contact area with loading, in agreement with the studies [46, 48].

Table 3 The maximum and mean FE-computed contact stresses in the tibial surface for the three loading conditions under study.
Legend: D – Dorsiflexion; N – Neutral; PF – Plantarflexion.

Loading condition	Contact stress (MPa) according to the position			
		D	N	PF
Axial force – 600 N	Mean	1.10	1.15	1.24
	Maximum	3.52	3.95	4.33
Axial force – 1600 N, 600 N, 400 N	Mean	2.17	1.15	0.95
	Maximum	6.16	3.95	3.61
Concentrated force + Torque	Mean	2.42	1.23	1.20
	Maximum	7.38	3.22	3.81

Regarding the magnitude of contact stress, using the same axial force for the three positions under study, the maximum and mean contact stresses increased from the dorsiflexion to plantarflexion positions, which was also observed in [46]. This feature was not found for the other two loading conditions because it was possible to identify an increasing contact stresses with loading – also reported in [46] – and so the higher magnitude of the loads applied in dorsiflexion position resulted in higher mean and maximum contact stresses. Furthermore, in the literature there is rare data describing the contact pattern on the tibial surface. Only a recent study of Anderson *et al.* [47] presents the FE-computed contact stress distribution in the tibial surface with the ankle in neutral position and using an axial load of 600 N. This study was conducted to determine the agreement between experimental and FE-computed results of contact stress distribution in the ankle joint. The FE-computed results of the present study show good comparison among the global magnitude of the contact stresses reported by Anderson *et al.* [47], as shown in Table 4.

Table 4 Comparison of the contact stresses reported in the study of Anderson *et al.* [47] and the FE results of the present study.

Source	Method	Maximum contact stress (MPa)	Mean contact stress (MPa)
Anderson <i>et al.</i> [47]	FEM	3.74 (ankle 1)	2.02 (ankle 1)
		2.74 (ankle 2)	1.36 (ankle 2)
	Tekscan	3.69 (ankle 1)	1.96 (ankle 1)
		2.92 (ankle 2)	1.15 (ankle 2)
Present study	FEM	3.95	1.15

To conclude, the analysis of the contact stress distribution is not the focus of this work and therefore, besides the limitations of this study, these results show reasonable comparison and are, for the most part, consistent with previous studies. Thus, this validation establishes confidence in results from the FE models.

4.2. Contact Stress Distribution in the Polyethylene Component

Preliminary Test

Firstly, the contact stress distribution was investigated in the polyethylene component's surface that contacts with the talar component of the Agility™ prosthesis, taking into account the old and new talar component designs. Then, the contact stresses were also determined for the polyethylene component's upper and lower surfaces of the S.T.A.R.™ prosthesis. This was done considering only an axial

force of 600 N with respect to the neutral position. Table 5 presents the maximum and mean FE-computed contact stresses in the polyethylene component's surfaces that contact with the old and new talar component designs of Agility™ prosthesis and with the tibial and talar components of the S.T.A.R.™ prosthesis.

Table 5 The maximum and mean FE-computed contact stresses in the polyethylene component's surfaces that contact with the old and new talar component designs of Agility™ prosthesis and with the tibial and talar components of the S.T.A.R.™ prosthesis, considering only an axial force of 600 N with respect to the neutral position.

Model	Agility™ (the old talar comp. design)	Agility™ (the new talar comp. design)	S.T.A.R.™ (talar comp.)	S.T.A.R.™ (tibial comp.)
Mean contact stress (MPa)	17.59	5.32	3.07	2.03
Maximum contact stress (MPa)	68.81	31.75	9.74	5.10

As expected, the wider shape of the new talar component design of Agility™ prosthesis at the posterior edge and the increased contact area provided by it led to a decrease of both the maximum and mean FE-computed contact stresses in the polyethylene component's surface. In particular, the mean contact stress decreased from 17.59 MPa (using the old design) to 5.32 MPa (using the new design) while the maximum contact stress decreased from 68.81 MPa (using the old design) to 31.75 MPa (using the new design). At first sight, the contact stresses calculated for the old talar component design seem unreasonably high. However, it is important to mention that three times larger stresses at the Agility™ prosthesis (considering the old design) than at the S.T.A.R.™ prosthesis were estimated in [49], which may confirm the great difference observed in this study. To conclude, these results indicate that the new talar component design has better performance than the old design, and as result, only the new talar component design was considered in a more detailed analysis of the contact stresses, as described below.

With the results from preliminary test in mind, the FE-computed contact stress distributions in the polyethylene component's surfaces for Agility™ (considering only the new talar component design) and S.T.A.R.™ prostheses and for dorsiflexion, neutral and plantarflexion positions are displayed in Figure 4. Once again, as done for the intact ankle joint, three loading conditions were considered in this study. For reasons of synthesis, only the results when considering an axial force of 600 N to the three positions are shown (the other results were similar).

Besides not shown here, the problem of edge-loading was evident in Agility™ prosthesis for the three loading conditions, and also for S.T.A.R.™ prosthesis in some loading conditions. This problem have been reported in several studies [10, 13, 50, 51]. In fact, in spite of the fact that the S.T.A.R.™ is a fully

congruent prosthesis, a non-uniform contact stress distribution was observed in the polyethylene component's surfaces, as also reported in [49, 52].

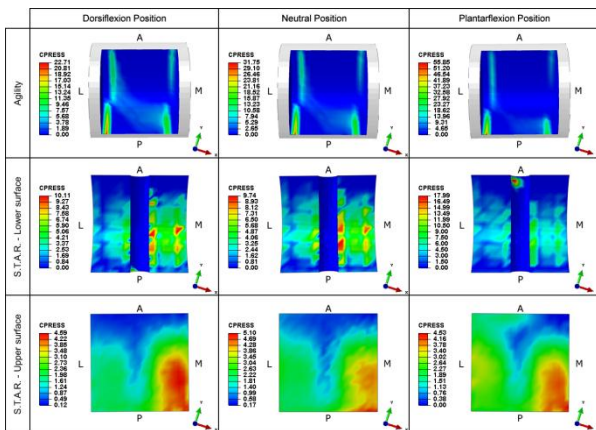


Figure 4 Inferior view of the polyethylene component's lower surfaces that articulate with the talar component of the Agility™ and S.T.A.R.™ prostheses and also the superior view of the polyethylene component's upper surface that articulates with the tibial component of the S.T.A.R.™ prosthesis, overlaid with FE-computed contact stresses (MPa) for the dorsiflexion, neutral and plantarflexion positions, considering only an axial force of 600 N to the three positions. Legend: A – Anterior; P – Posterior; L – Lateral; M – Medial. Software used: ABAQUS®.

A quantitative analysis of the contact stresses was also performed. The maximum and mean FE-computed contact stresses in the polyethylene component's surfaces for Agility™ and S.T.A.R.™ prostheses are summarized in Tables 6, 7 and 8.

Table 6 The maximum and mean FE-computed contact stresses in the polyethylene component's lower surface of the Agility™ prosthesis for the three loading conditions under study. Legend: D – Dorsiflexion; N – Neutral; PF – Plantarflexion.

Loading condition		Contact stress (MPa) according to the position		
		D	N	PF
Axial force – 600 N	Mean	4.20	5.32	8.21
	Maximum	22.71	31.75	55.85
Axial force – 1600 N, 600 N, 400 N	Mean	9.79	5.32	6.61
	Maximum	52.08	31.75	40.33
Concentrated force + Torque	Mean	15.82	3.39	2.97
	Maximum	63.45	14.74	17.92

Table 7 The maximum and mean FE-computed contact stresses in the polyethylene component's lower surface of the S.T.A.R.™ prosthesis for the three loading conditions under study. Legend: D – Dorsiflexion; N – Neutral; PF – Plantarflexion.

Loading condition		Contact stress (MPa) according to the position		
		D	N	PF
Axial force – 600 N	Mean	3.09	3.07	3.63
	Maximum	10.11	9.74	17.99
Axial force – 1600 N, 600 N, 400 N	Mean	7.21	3.07	2.45
	Maximum	25.87	9.74	10.73
Concentrated force + Torque	Mean	7.38	7.65	6.13
	Maximum	23.05	25.26	20.63

Table 8 The maximum and mean FE-computed contact stresses in the polyethylene component's upper surface of the S.T.A.R.™ prosthesis for the three loading conditions under study. Legend: D – Dorsiflexion; N – Neutral; PF – Plantarflexion.

Loading condition		Contact stress (MPa) according to the position		
		D	N	PF
Axial force – 600 N	Mean	1.86	2.03	2.12
	Maximum	4.59	5.10	4.53
Axial force – 1600 N, 600 N, 400 N	Mean	4.92	2.03	1.44
	Maximum	10.30	5.10	3.03
Concentrated force + Torque	Mean	5.17	5.96	5.15
	Maximum	10.82	13.34	12.36

The reported maximum and mean contact stresses from the literature are in the range of 5.7-36 MPa and 5.6-23 MPa, respectively. In the present study, for Agility™ prosthesis, the maximum contact stresses were in the range of 14.74-63.45 MPa, while the mean contact stresses were in the range of 2.97-15.82. On the other hand, for S.T.A.R.™ prosthesis these values decreased: maximum contact stresses were in the range of 9.74-25.87 MPa (lower surface) and 3.03-13.34 MPa (upper surface), while the mean contact stresses were in the range of 2.45-7.65 (lower surface) and 1.44-5.96 MPa (upper surface).

The comparison of the present results with previous studies from the literature is difficult because of the different designs analysed, the different boundary and loading conditions applied, etc. Larger values of the contact stresses were observed in the present study, mostly for the Agility™ prosthesis. The main reason is probably related to the loading conditions considered in the present study. For the first time, at the present state of knowledge, a 3-D concentrated force and an internal-external torque were applied in a contact stress analysis of a replaced ankle and in particular, for the Agility™ and S.T.A.R.™ prostheses. As it has been confirmed, there is an increased contact stress with loading, and so the larger values observed in the present study may be related to that fact. In general, the FE-computed contact stresses in the present study show good comparison among the reported contact stresses from the literature.

Furthermore, some studies [10, 53] have indicated that to achieve a successful TAA the contact stresses should not exceed 10 MPa in polyethylene component. However, both prostheses exceeded the recommended value for the polyethylene component (10 MPa) and its compressive yield point (13-25 MPa [10]). In fact, these prostheses still have some untested features and the optimal articulation configuration is currently not known. On the one hand, mobile-bearing designs (such as S.T.A.R.™) theoretically offer less wear and loosening because of full conformity and minimal constraint, respectively. On the other hand, fixed-bearing designs (such as Agility™) avoid the dislocation of the polyethylene component and the potential increased wear from a second articulation/contact surface.

4.3. Internal Stress Distribution in the Talus

The internal stress distribution was investigated in the talus for the intact, TAA+Agility™ (including the old and new talar component designs) and TAA+S.T.A.R.™ models, considering only an axial force of 600 N with respect to the neutral position. The results are shown in Figure 5.

By analysing the results, it is possible to notice that the intact talus distributes stresses evenly throughout the bone and that there is a preferential area for the transmission of force from talus to the calcaneus. After the insertion of both prostheses (taking into account the two talar components for Agility™) major changes occurred in the talus, in particular, in its internal stress distribution. There was an increase of

the magnitude of stresses in trabecular bone for the three models. When comparing the two talar components of Agility™ prosthesis, the wider shape of the new design at the posterior edge and the increased contact area provided by it led to a decrease of the maximum internal stresses in the talus. In particular, the Von Mises stresses decreased from 54.25 MPa (using the old design) to 40.96 MPa (using the new design). Moreover, the old design originated larger stresses at the posterior edge, which can explain the early loosening and subsidence of this component. In fact, clinically, the old design was noted to fail due to posterior subsidence, which is in accordance with the present results. These results show once again that the new talar component design has better performance than the old design.

Furthermore, when comparing the stress distribution in the talus using the new talar component design of Agility™ prosthesis and the talar component of S.T.A.R.™ prosthesis, it is possible to identify an improvement in the stress distribution in the case of S.T.A.R.™, despite the slight increase in stresses at the anterior medial side of the talus. In the case of Agility™ a clearly marked area of larger stresses around the prosthesis was identified, despite not being so significant when comparing with the area originated by the old talar component design.

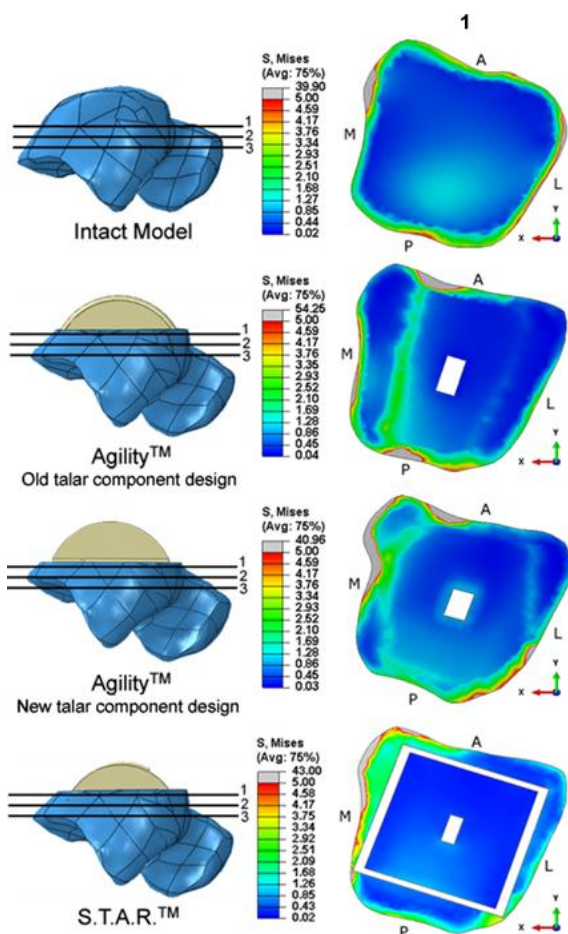


Figure 5 The Von Mises stress distribution (MPa) in the talus for the intact, TAA+Agility™ (including the old and new talar component designs) and TAA+S.T.A.R.™ models, considering only an axial force of 600 N with respect to the neutral position. The cut was done in the transverse plane near the surface where the talar component is place (superior view). Legend: A – Anterior; P – Posterior; L – Lateral; M – Medial. Software used: ABAQUS®.

This was also expected since the S.T.A.R.™ is a three-component, mobile-bearing design, which means that it is at the same time a congruent and unconstrained prosthesis (and thus providing full mobility), whereas Agility™ is a two-component, fixed-bearing design, i.e., it is a partially conforming and semiconstrained prosthesis, which may originate high axial and shear constrains at the bone-prosthesis interface.

To conclude, the present results agree that excessive bone resection results in the prosthesis being seated on trabecular bone that may not support the forces at the ankle, which consequently may contribute to early loosening and subsidence of the talar component, as also reported in [54, 55]. Thus, minimal bone resection is required in order to remain firm the bone-prosthesis interface.

4.4. Bone Remodeling of the Intact Bones: Talus and Tibia

The tibia and talus are the two bones considered as design area in the bone remodeling simulations. Using the intact model of the AJC, several bone remodeling computer simulations were performed, assuming different values for k and m , to assess which ones best fit the real bone density distribution of the talus and tibia (physiological state). The most appropriate values for the parameters k and m were chosen from the comparison of the bone density distributions resulting from the bone remodeling computer simulations and the CT scan images (qualitative analysis). For reasons of synthesis, only the best result of the computer simulations with $k = 0,007 \text{ N/mm}^2$ and $m = 2$ is presented in Figure 6.

The model converged to a solution with relatively high similarity to the morphology of the tibia, when comparing to the CT scan images. It is possible to observe an inner area of lower relative densities, which correspond to trabecular bone, surrounded by an external layer of higher relative densities, which correspond to cortical bone. In particular, the cortical layer is thicker in the diaphysis and becomes thinner toward one extremity. However, like CT scan images show (frontal plane view), the cortical layer is thicker in the diaphysis and becomes thinner toward both extremities but the present results could not simulate perfectly well one of the extremities. Moreover, as visible in sagittal plane, there is a thick cortical layer in the anterior side and a thin cortical layer in the posterior side of the tibia, and the anterior and posterior sides should be more uniform, as CT scan images show (sagittal plane view). As far as talus is concerned, it is important to notice that navicular – the bone in direct contact with the anterior side of the talus – was not included in the model and due to that fact, the loads that are originated in the talus from the contact surfaces of the talus and navicular are not observed in the present model. With this limitation is mind, it is easy to understand the “black” area (very low densities) present in the anterior side of the talus (sagittal plane view), which was visible in all bone remodeling computer simulations. This result from the

assumption that bone adapts itself according to the applied loads and so, if there are no loads, there is no bone formation. Besides this, it is also visible in the sagittal plane – considering both CT scan images and present results – a concentrated area in the middle and distal side of talus that corresponds to the area of force transmission to the calcaneus. On the other hand, in the frontal plane it is also noticeable small “black” areas (very low densities) that are not visible in the CT scan images. This could be result of the ligaments’ modeling, i.e., the real attachment sites for the ligaments into the talus may occupy a larger area than the one that was considered, which would have a direct impact on the bone remodeling process. With this in mind, the “white” area (very high densities) also visible in the medial side of the frontal plane may have been caused by a concentrated attachment area of a particular ligament into the talus. The aforementioned negative points can be improved in future works.

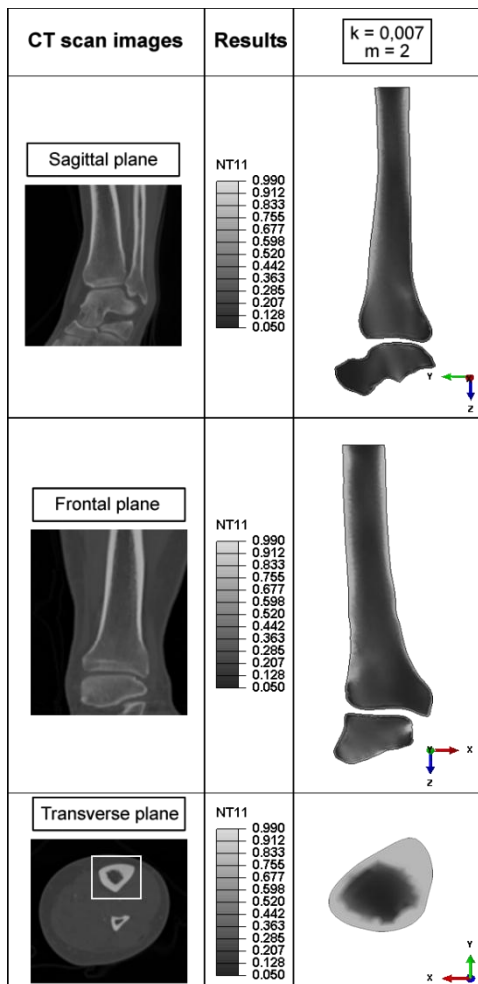


Figure 6 Comparison of the bone density distributions resulting from the bone remodeling computer simulations (after 100 iterations) and the CT scan images. Software used: ABAQUS®.

Besides not shown here, the process has reached the desired convergence (the change in bone mass stabilized) within the number of iterations considered. This means that the solution of the model converged towards an equilibrium state between successive bone formation and bone resorption events.

To conclude, it is very important understand the bone remodeling process prior to the insertion of a prosthesis, and so the validation of the bone remodeling models obtained for tibia and talus is also an important step before analysing the effects of the ankle prostheses on the bones. However, if the aim of the study was to analyse the importance on the bone remodeling process of inserting an ankle prosthesis into the AJC, that can be done by considering the final bone density distribution obtained from the model of the intact AJC as the initial bone density distribution of the model of the AJC after the insertion of the prosthesis. This way, it is possible to analyse only the changes caused by the insertion of the prosthesis. This was the strategy applied in the present study.

4.5. Bone Remodeling of the Talus and Tibia after the TAA

As explained before, the initial density distributions of the tibia and talus in the TAA+Agility™ and TAA+S.T.A.R.™ models correspond to the final density distributions of the tibia and talus in the intact model. Thus, tibia and talus start from an initial situation with greater resemblance to reality and, consequently, to clinical scenario. The results of TAA+Agility™ and TAA+S.T.A.R.™ models are presented in Figures 7 and 8. In order to analyse the evolution of each of the bone density distributions, the physiological and the initial states are also presented. It is important to mention that bone remodeling processes in the prosthetic tibia and talus occur mainly in the metaphysis/epiphysis, where the prosthesis is implanted. Hence, the changes in bone density distribution are only analysed in that region.

Regarding the TAA+Agility™ model, the present results showed a decrease in density in the medial region of the talus beneath the talar component, which could be associated with stress shielding effect. However, further investigation is still needed to confirm these results. Regarding the TAA+S.T.A.R.™ model, the present results showed an increase in density above the two raised cylindrical barrels, which was also reported by in [19]. Moreover, in [19] was also observed a decrease in density centrally above the tibial component, which was not visible in the present results. Instead, a decrease of bone mass was visible in the lateral region of the distal tibia. Besides this, both results showed that forces are transmitted from the two raised cylindrical barrels into the bone, which may lead to stress shielding in some areas near these two structures. This was also pointed out by Hintermann in [56]. Moreover, a bone mass loss was also observed in the lateral region beneath the talar component. This stress shielding effect may contribute to loosening and subsidence of the tibial and/or talar components, often reported in clinical studies. Although these are preliminary results, a relatively good agreement was achieved between these results and the results of the study of Boughecha *et al.* [19] for the S.T.A.R.™ prosthesis.

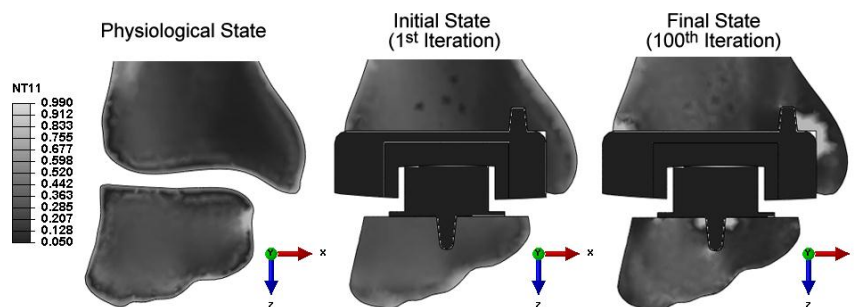


Figure 7 Bone density distributions in the tibia and talus before and after the insertion of Agility™ prosthesis (frontal plane view). Software used: ABAQUS®.

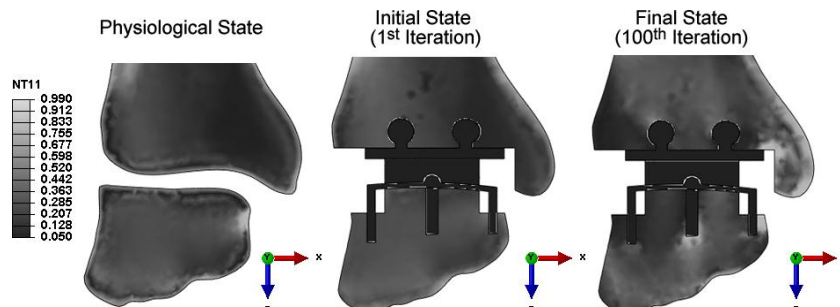


Figure 8 Bone density distributions in the tibia and talus before and after the insertion of S.T.A.R.™ prosthesis (frontal plane view). Software used: ABAQUS®.

5. Conclusions and Future Directions

This work analysed the internal and contact stress distributions and the bone remodeling of the AJC before and after a TAA using two different prostheses, Agility™ and S.T.A.R.™.

The contact stress distribution in the polyethylene component of both prostheses was evaluated. The results indicate that the new talar component design has better performance than the old design. Also, the problem of edge-loading was observed in both prostheses. Moreover, both prostheses (especially Agility™) exceeded the contact stress recommended for the polyethylene component (10 MPa) and its compressive yield point (13-25 MPa). In fact, these prostheses still have some untested features and the optimal articulation configuration is currently not known. Then, the internal stress distribution was investigated in the talus for the three models under study. The results showed that stresses increased near the resected surfaces after the insertion of both prostheses. In particular, there was an increase of the magnitude of stresses in trabecular bone. The present results agree that excessive bone resection results in the prosthesis being seated on trabecular bone that may not support the forces at the ankle, which consequently may contribute to early loosening and subsidence of the talar component. Thus, minimal bone resection is required in order to remain firm the bone-prosthesis interface. Lastly, the bone remodeling process was investigated in the talus and tibia. The model converged to a solution with relatively high similarity to the morphology of the tibia, reproducing the behaviour of the real bone, but with less similarity to the morphology of the talus. Then, in order to evaluate the changes in the bone remodeling process that occur in the tibia and talus after a TAA, the final density distributions of the tibia and talus in

the intact model were considered as the initial density distributions of the tibia and talus in the TAA+Agility™ and TAA+S.T.A.R.™ models. As result, both prostheses showed evidences that may lead to stress shielding effect. However, further investigation is still needed to confirm these results.

Among the main limitations of the present study are the loading conditions considered in the models. In the best case, only three different static load cases were applied to each model. These selected load cases correspond to discrete times of the stance phase of gait and are considered representative of the range of loads developed during the stance phase. However, in reality more complex loading conditions can be expected. In fact, there are not enough computational resources to consider the entire range of loads of the stance phase of gait. Moreover, there is no information in the literature about the muscular forces, and so they were not included in the present work. In future works, force patterns derived from multibody simulations should be incorporated into the FE models in order to examine the influence of the muscular forces. The research in TAA would benefit from further *in vivo* studies of the forces acting across the ankle joint, such as instrumented, telemeterized prosthesis. Also, further analysis of other gait activities, such as chair climbing, squat, among others, are required.

BIBLIOGRAPHY

- [1] van den Heuvel, A., Van Bouwel, S., and Dereymaeker, G., *Total ankle replacement. Design evolution and results*. Acta Orthop Belg, 2010. **76**(2): p. 150-61.
- [2] *Centers for Disease Control and Prevention™* [cited 2013 February 16]; Available from: <http://www.cdc.gov/arthritis/basics/osteoarthritis.htm>.

- [3] American Academy of Orthopaedic Surgeons. [cited 2013 February 26]; Available from: <http://orthoinfo.aaos.org/topic.cfm?topic=A00208>.
- [4] Espinosa, N. and Klammmer, G., *Treatment of ankle osteoarthritis: arthrodesis versus total ankle replacement*. European Journal of Trauma and Emergency Surgery, 2010. **36**(6): p. 525-535.
- [5] American Orthopaedic Foot & Ankle Society®. [cited 2013 February 27]; Available from: http://www.aofas.org/medical-community/health-policy/Documents/TAR_0809.pdf.
- [6] Tooms, R.E., *Arthroplasty of ankle and knee*. In: Crenshaw, A.H. (Ed.), *Campbell's Operative Orthopedics*. C.V. Mosby Company, St.Lois, 1987: p. 1145-1150.
- [7] Buechel, F.F., Sr., Buechel, F.F., Jr., and Pappas, M.J., *Ten-year evaluation of cementless Buechel-Pappas meniscal bearing total ankle replacement*. Foot Ankle Int, 2003. **24**(6): p. 462-72.
- [8] Buechel, F.F., Sr., Buechel, F.F., Jr., and Pappas, M.J., *Twenty-year evaluation of cementless mobile-bearing total ankle replacements*. Clin Orthop Relat Res, 2004(424): p. 19-26.
- [9] Feldman, M.H. and Rockwood, J., *Total ankle arthroplasty: a review of 11 current ankle implants*. Clin Podiatr Med Surg, 2004. **21**(3): p. 393-406, vii.
- [10] Gill, L.H., *Challenges in total ankle arthroplasty*. Foot Ankle Int, 2004. **25**(4): p. 195-207.
- [11] Knecht, S.I., Estin, M., Callaghan, J.J., Zimmerman, M.B., Alliman, K.J., Alvine, F.G., and Saltzman, C.L., *The Agility total ankle arthroplasty. Seven to sixteen-year follow-up*. J Bone Joint Surg Am, 2004. **86-A**(6): p. 1161-71.
- [12] Pyevich, M.T., Saltzman, C.L., Callaghan, J.J., and Alvine, F.G., *Total ankle arthroplasty: a unique design - Two to twelve-year follow-up*. Journal of Bone and Joint Surgery-American Volume, 1998. **80A**(10): p. 1410-1420.
- [13] Wood, P.L. and Deakin, S., *Total ankle replacement. The results in 200 ankles*. J Bone Joint Surg Br, 2003. **85**(3): p. 334-41.
- [14] Easley, M.E., Vertullo, C.J., Urban, W.C., and Nunley, J.A., *Total ankle arthroplasty*. J Am Acad Orthop Surg, 2002. **10**(3): p. 157-67.
- [15] Giannini, S., Leardini, A., and O'Connor, J.J., *Total ankle replacement: review of the designs and of the current status*. Foot and Ankle Surgery, 2000. **6**(2): p. 77-88.
- [16] Steck, J.K. and Anderson, J.B., *Total ankle arthroplasty: indications and avoiding complications*. Clin Podiatr Med Surg, 2009. **26**(2): p. 303-24.
- [17] Vickerstaff, J.A., Miles, A.W., and Cunningham, J.L., *A brief history of total ankle replacement and a review of the current status*. Med Eng Phys, 2007. **29**(10): p. 1056-64.
- [18] Relvas, C., Fonseca, J., Amado, P., Castro, P., Ramos, A., Completo, A., and Simões, J., *Desenvolvimento de uma prótese do tornozelo: desafio projectual*, in *4º Congresso Nacional de Biomecânica*. 2001: Coimbra.
- [19] Bougoucha, A., Weigel, N., Behrens, B., Stukenborg-Colsman, C., and Waizy, H., *Numerical simulation of strain-adaptive bone remodeling in the ankle joint*. BioMedical Engineering OnLine, 2011. **10**(58).
- [20] Michael, J.M., Golshani, A., Gargac, S., and Goswami, T., *Biomechanics of the ankle joint and clinical outcomes of total ankle replacement*. J Mech Behav Biomed Mater, 2008. **1**(4): p. 276-94.
- [21] Leardini, A., O'Connor, J.J., Catani, F., and Giannini, S., *A geometric model of the human ankle joint*. J Biomech, 1999. **32**(6): p. 585-91.
- [22] Sammarco, G.J. and Hockenbury, R.T., *Chapter 9 - Biomechanics of the Foot and Ankle*, in *Basic Biomechanics of the Musculoskeletal System*. Lippincott Williams & Wilkins.
- [23] Komistek, R.D., Stiehl, J.B., Buechel, F.F., Northcut, E.J., and Hajner, M.E., *A determination of ankle kinematics using fluoroscopy*. Foot Ankle Int, 2000. **21**(4): p. 343-50.
- [24] Hintermann, B., *Chapter 5 - History of Total Ankle Arthroplasty*, in *Total Ankle Arthroplasty - Historical overview, current concepts and future perspectives*. 2005, SpringerWienNewYork.
- [25] Fernandes, P., Rodrigues, H., and Jacobs, C., *A Model of Bone Adaptation Using a Global Optimisation Criterion Based on the Trajectory Theory of Wolff*. Comput Methods Biomech Biomed Engin, 1999. **2**(2): p. 125-138.
- [26] Fernandes, P.R., Guedes, J.M., and Rodrigues, H., *Topology Optimization of 3D Linear Elastic Structures*. Computers & Structures, 1999. **73**: p. 583-594.
- [27] Folgado, J., *Modelos Computacionais para Análise e Projecto de Próteses Ortopédicas - Ph.D. Thesis*. 2004, Instituto Superior Técnico: Lisbon.
- [28] Folgado, J., Fernandes, P.R., and Rodrigues, H., *Topology Optimization of Three-Dimensional Structures under Contact Conditions*. IDMEC-IST: Lisbon.
- [29] Guedes, J.M. and Kikuchi, N., *Preprocessing and postprocessing for materials based on the homogenization method with adaptive finite element methods*. Computer methods in applied mechanics and engineering (Elsevier Science Publishers) 1990. **83**: p. 143-198.
- [30] VAKHUM project. [cited 2012 1st March]; Available from: <http://www.ulb.ac.be/project/vakhum/>.
- [31] "Agility Ankle Surgical Technique" – DePuy Orthopaedics, Inc. [cited 2013 4th March]; Available from: <http://www.depuy.com/healthcare-professionals/product-details/agility-ip-total-ankle-system>.
- [32] "STAR Instruments Guide" – Small Bone Innovations, Inc. [cited 2013 4th March]; Available from: <http://www.star-ankle.com/>.
- [33] "Agility Ankle Primary Revision" – DePuy Orthopaedics, Inc. [cited 2013 4th March]; Available from: <http://www.depuy.com/healthcare-professionals/product-details/agility-ip-total-ankle-system>.
- [34] "STAR Surgical Technique" – Small Bone Innovations, Inc. [cited 2013 4th March]; Available from: <http://www.star-ankle.com/>.
- [35] Reggiani, B., Leardini, A., Corazza, F., and Taylor, M., *Finite element analysis of a total ankle replacement during the stance phase of gait*. Journal of Biomechanics, 2006. **39**(8): p. 1435-1443.
- [36] Corazza, F., O'Connor, J.J., Leardini, A., and Parenti Castelli, V., *Ligament fibre recruitment and forces for the anterior drawer test at the human ankle joint*. J Biomech, 2003. **36**(3): p. 363-72.
- [37] Pankovich, A.M. and Shivaram, M.S., *Anatomical basis of variability in injuries of the medial malleolus and the deltoid ligament. I. Anatomical studies*. Acta Orthop Scand, 1979. **50**(2): p. 217-23.
- [38] Cowin, C.S., *The mechanical properties of cortical bone tissue*. In: Cowin, C.S. (Ed.), *Bone Mechanics*, CRC, Florida, 1991.
- [39] Yamada, H., *Strength of Biological Materials*. Williams and Wilkins, Baltimore, 1970.
- [40] Jensen, N.C., Hvid, I., and Kroner, K., *Strength pattern of cancellous bone at the ankle joint*. Eng Med, 1988. **17**(2): p. 71-6.
- [41] Athanasiou, K.A., Liu, G.T., Lavery, L.A., Lanctot, D.R., and Schenck, R.C., Jr., *Biomechanical topography of human articular cartilage in the first metatarsophalangeal joint*. Clin Orthop Relat Res, 1998(348): p. 269-81.
- [42] Lewis, G. and Austin, G.E., *A Finite Element Analysis Study of Static Stresses in a Biomaterial Implant*. Innovations and Technology in Biology and Medicine, 1994. **15**(5): p. 634-644.
- [43] DeHeer, D.C. and Hillberry, B.M., *The Effect of Thickness and Nonlinear Material Behaviour on Contact Stresses in Polyethylene Tibial Components*, in *In 38th Annual Meeting of the ORS*. 1992: p. 327.
- [44] Cheung, J. and Zhang, M., *Finite Element Modeling of the Human Foot and Footwear*, in *ABAQUS Users' Conference*. 2006.
- [45] Serway, R.A. *Física*. 1992.
- [46] Calhoun, J.H., Li, F., Ledbetter, B.R., and Viegas, S.F., *A comprehensive study of pressure distribution in the ankle joint with inversion and eversion*. Foot Ankle Int, 1994. **15**(3): p. 125-33.
- [47] Anderson, D.D., Goldsworthy, J.K., Li, W., James Rudert, M., Tochigi, Y., and Brown, T.D., *Physical validation of a patient-specific contact finite element model of the ankle*. J Biomech, 2007. **40**(8): p. 1662-9.
- [48] Kimizuka, M., Kurosawa, H., and Fukubayashi, T., *Load-bearing pattern of the ankle joint. Contact area and pressure distribution*. Arch Orthop Trauma Surg, 1980. **96**(1): p. 45-9.
- [49] Mcliff, T.E., Horton, G.A., Saltzman, C.L., and Brown, T.D., *Finite element modelling of total ankle replacement for constraint and stress analysis*. In: Proceedings of the Fourth World Congress in Biomechanics, Calgary, 4-9 August 2002, 2002.
- [50] Wood, P.L., *Experience with the STAR ankle arthroplasty at Wrightington Hospital, UK*. Foot Ankle Clin, 2002. **7**(4): p. 755-64, vii.
- [51] Wood, P.L., *Which ankle prosthesis?* Presented at the 29th Annual Meeting of the British Orthopaedic Foot Surgery Society, Cumbria, UK, May 1 – 3, 2003.
- [52] Mcliff, T.E., *Design factors affecting the contact stress patterns in a contemporary mobile bearing total ankle replacement*. In: Proceedings of the Fourth World Congress in Biomechanics, Calgary, 4-9 August, 2002.
- [53] Pappas, M.J. and Buechel, F.F., *Biomechanics and design rationale: The Buechel-Pappas ankle replacement system*.
- [54] Calderale, P.M., Garro, A., Barbiero, R., Fasolio, G., and Pipino, F., *Biomechanical design of the total ankle prosthesis*. Eng Med, 1983. **12**(2): p. 69-80.
- [55] Kempson, G.E., Freeman, M.A., and Tuke, M.A., *Engineering considerations in the design of an ankle joint*. Biomed Eng, 1975. **10**(5): p. 166-71, 80.
- [56] Hintermann, B., *Endoprothetik des Sprunggelenks. Historischer Überblick, aktuelle Therapiekonzepte und Entwicklungen*. 2005: Wien New York, Springer Verlag.